Materials Today Bio 31 (2025) 101511

Contents lists available at ScienceDirect

Materials Today Bio

journal homepage: www.journals.elsevier.com/materials-today-bio

Injectable hydrogel regulates immune infiltration through physical and chemical synergy in the treatment of steroid-induced osteonecrosis of the femoral head

Zherui Fu [a,1], Yiwen Xu [b,1], Fangqi Xu [a], Haoyu Zhou [a], Na Lin [c], Ning Zhang [b], Feng Lin [b,*]

[a] Department of Emergency, The First People's Hospital of Xiaoshan District, Xiaoshan Affiliated Hospital of Wenzhou Medical University, Hangzhou, 310000, PR China
[b] Department of Orthopaedic Surgery, The Second Affiliated Hospital, Zhejiang University School of Medicine, Orthopedics Research Institute of Zhejiang University, Key Laboratory of Motor System Disease Research and Precision Therapy of Zhejiang Province, Clinical Research Center of Motor System Disease of Zhejiang Province, Hangzhou, 310000, PR China
[c] Department of Orthopaedic Surgery, Children's Hospital, Zhejiang University School of Medicine, Hangzhou, 310000, PR China

ARTICLE INFO

Keywords:
Injectable hydrogel
Immune infiltration
Th17 cell
Steroid-induced
Osteonecrosis of the femoral head

ABSTRACT

The incidence of steroid-induced osteonecrosis of the femoral head (SONFH) is increasing annually; however, the underlying pathological mechanism remains unclear, which is an obstacle to its effective treatment. The negative effect of immune infiltration on the physiological activity of focal stem cells is one potential mechanism that has attracted attention. It is difficult to simulate the complex regulation of the interaction system between immune cells and stem cells using a single regulation method. In this study, we demonstrated that the immune infiltration of T helper 17 (Th17) cells plays an important role in the progression of SONFH. Based on this finding, we developed an injectable hydrogel system with both physical and chemical synergistic regulatory properties to enhance the activity of stem cells using electrical stimulation. This treatment was designed to prevent the infiltration of Th17 cells by regulating the physiological function of stem cells and blocking the negative effect of Th17 cells on stem cells pharmacologically. Thus, the dual synergistic regulation of immune infiltration at the lesion site of SONFH enhanced the physiological activity and function of the stem cells, thereby improving the therapeutic effect of SONFH. This hydrogel system provides insight for the future development of multifactorial regulatory systems and provides a strategy for the treatment of SONFH.

1. Introduction

With the development of medicine, hormones are becoming increasingly used in clinical practice, and steroid-induced osteonecrosis of the femoral head (SONFH) is occurring more frequently. The incidence of SONFH has now exceeded that of traumatic osteonecrosis of the femoral head. The underlying mechanism of SONFH is unclear, which is a significant treatment challenge [1–3]. Surgery is the standard treatment for SONFH; however, the treatment is considerably expensive and is quite painful to the patient [4–6]. In recent years, the development of injectable biomaterials has enabled the nonsurgical treatment of this disease, thereby substantially reducing the economic pressure and physical pain for patients undergoing surgery [7–9]. Therefore, the development of injectable biomaterials for the treatment of SONFH is expected to benefit patients and society.

The development of a hydrogel system that can regulate the physiological activity and function of stem cells represents a strategy for the treatment of SONFH. For example, Liu et al. [10] developed a selenium nanoparticle/carboxymethyl chitosan/alginate antioxidant hydrogel that can remove lesions caused by reactive oxygen species. It can regulate the osteogenesis capacity of stem cells, vascular differentiation, and ameliorate SONFH. Various biomaterials have been developed to enhance the physiological activity and function of stem cells [11–13]; however, the pathological microenvironment in which the stem cells reside is complex and filled with various immune cells. The negative effects of immune cells on stem cells must be considered [14–16]. Thus, examining the relationship between SONFH and immune infiltration is an important part of SONFH treatment. It can also provide a theoretical basis for the development of biomaterials that regulate immune infiltration.

* Corresponding author.
E-mail address: linfeng2023@zju.edu.cn (F. Lin).
[1] These authors contributed equally to this work.

https://doi.org/10.1016/j.mtbio.2025.101511
Received 7 November 2024; Received in revised form 13 January 2025; Accepted 19 January 2025
Available online 21 January 2025

There have been many studies on the progression of SONFH induced by immune cells. For example, in SONFH animal models, neutrophils and macrophages are increased in the osteonecrosis tissue. Necrotic bone can regulate the inflammatory response by activating Toll-like receptor 4 (TLR4) and upregulating downstream transcription factors, including nuclear factor-κB (NF-κB) and monocyte chemoattractant protein 1 (MCP-1) to stimulate macrophages [17]. The number of monocytes in bone marrow samples from patients with SONFH was found to be three-fold higher compared with that of other causes [18]. Glucocorticoids can directly act on monocytes *in vivo* and *in vitro*, induce their expansion, and promote their differentiation into osteoclasts by increasing cytokine signaling. They exert an inflammatory response and bone fragmentation capacity, which eventually leads to bone loss and reduced blood supply [19]. Therefore, regulating immune infiltration using the hydrogel system will markedly improve its efficacy for the treatment of SONFH.

Significant progress has been made in the field of medical biomaterials for regulating immune infiltration through chemical and physical methods. For example, Wu et al. [20] used piezoelectric material to prepare a biomaterial exhibiting electrical stimulation for anti-inflammatory polarization of macrophages and to promote bone repair. Xiao et al. [21] constructed immune cell-mobilized hydrogel microspheres loaded with chemokines, macrophage antibodies, and engineered cell membrane vesicles. Using these chemical entities, the recruitment and activation of macrophages at the lesion site could be precisely regulated. Therefore, if these physical and chemical methods can be regulated synergistically, the immune infiltration of SONFH may be alleviated, which will greatly improve the treatment of SONFH.

In this study, we developed an injectable hydrogel system with both physical and chemical synergistic regulatory properties to enhance the physiological activity of stem cells using a physical method (electrical stimulation), prevent the infiltration of Th17 cells by regulating stem cell physiological function, and block the negative effect of Th17 cells on stem cells through a chemical method, thus achieving the synergistic regulation of immune infiltration into the lesion. Briefly, PLGA [poly (lactic-co-glycolic acid)]-PEG (polyethylene glycol)-PLGA was used to construct a thermosensitive hydrogel carrier. The hydrogel was liquid at room temperature with excellent injectability. When injected into the lesion site of the femoral head, the hydrogel was stimulated by body temperature to form a solid, thereby achieving long-term indwelling for sustained treatment. Subsequently, we used electrospinning to construct polylactic acid (PLLA) nanofibrils with piezoelectric properties and thin-film hydration to construct chemically loaded nanoliposomes. The combination of the three functional components forms an injectable hydrogel system that exhibits synergistic physical and chemical regulation. Under the stimulation of ultrasound *in vitro*, the piezoelectric nanofibers in the hydrogel system generated a microcurrent that stimulates the lesion stem cells. Electrical stimulation of stem cells can significantly enhance their physiological activity by improving respiratory chain function and osteogenic differentiation ability, which contributes to the repair and regeneration of lesions. Electrically stimulated stem cells can reduce the secretion of Th17 cell-related chemokines, thereby inhibiting the immune infiltration of Th17 cells. The hydrogel system can then release chemical inhibitors through nanoliposomes to inhibit the synthesis of interleukin-17 (IL-17) by Th17 cells, thereby inhibiting stem cell apoptosis induced by Th17. Finally, we observed that physical and chemical methods can synergistically regulate the negative effect of immune infiltration on SONFH, which is conducive to the repair and regeneration of SONFH lesions (Scheme 1). This hydrogel system provides insight into the development of multiple regulatory systems and presents a promising strategy for the treatment of SONFH.

2. Materials and methods

2.1. Bioinformatics analysis

The GSE123568 dataset was mined from public databases. The R package 'ggstatsplot' was used to analyze the differentially expressed

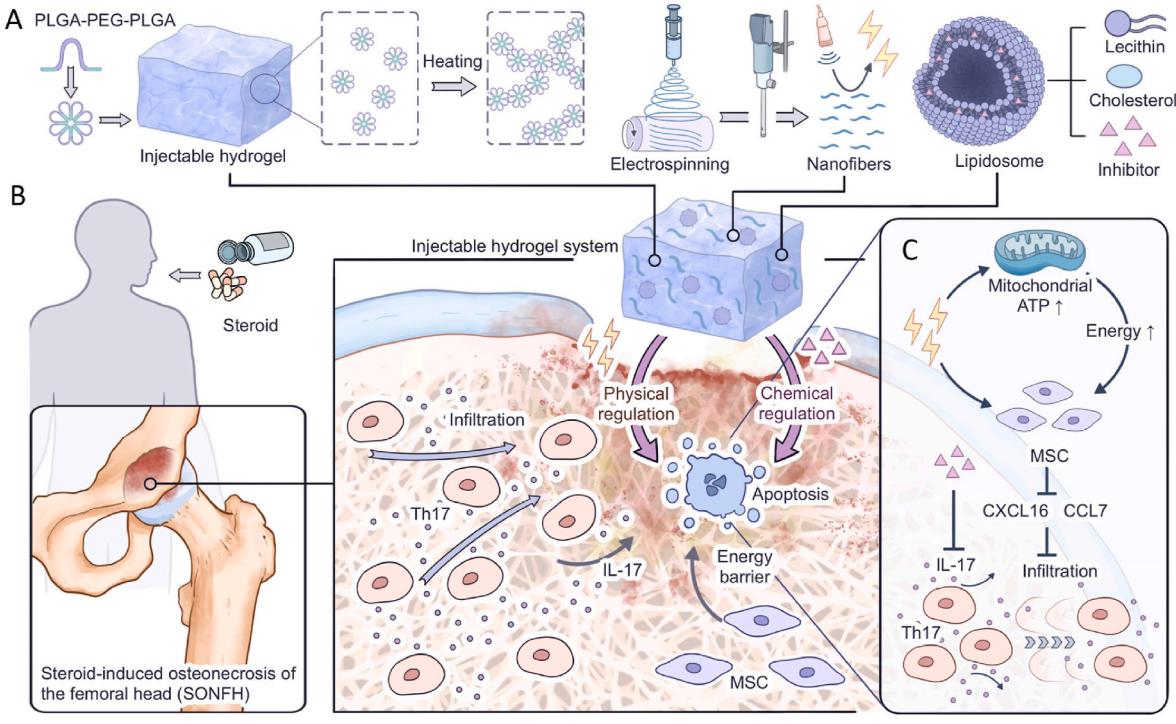

Scheme 1. Injectable hydrogel regulates immune infiltration through physical and chemical synergy in the treatment of SONFH. A) Construction of the injectable hydrogel system with physical and chemical dual regulation methods. B) The immune infiltration of Th17 cells and the physiological dysfunction of stem cells lead to the progression of SONFH. C) Physical (electrical stimulation) and chemical (IL-17 inhibitor) methods synergistically regulate Th17 cells and stem cells, effectively inhibit the apoptosis of stem cells, and promote the efficacy of SONFH treatment.

genes in the dataset. The obtained differential genes were subjected to biological enrichment pathway analysis (GO/KEGG pathway analysis, https://www.xiantaozi.com/), which sets the threshold at the screening, $P < 0.05$. The relative abundance of immune cell infiltration in steroid-induced osteonecrosis of the femoral head and the control group was analyzed by ssGSEA method. The R language 'clusterprofiler' package was used to analyze the parameters, and the default values were used.

2.2. Materials

Polyethylene glycol (PEG)-1500 was obtained from Aladdin Biochemical Technology Co., Ltd. (Shanghai, China). Glycolide (GA) and D, L-lactide (LA) were obtained from Ming Zhong Biotechnology Co., Ltd. (Hangzhou, China). Stannous octoate [Sn(Oct)2]. Poly-L-lactic acid (PLLA) were obtained from Yuanye Bio-Technology Co., Ltd. (Shanghai, China). IL-17 inhibitor (IL-17-IN-1) was obtained from MCE Co., Ltd. Cholesterol and lecithin (from egg yolk) were obtained from Sangon Biotech (Shanghai) Co., Ltd. All other reagents are described in detail in the text.

2.3. Preparation of injectable hydrogels

Firstly, electro spun films were prepared using the electrospinning instrument (SS-X1, Yongkang Leye Technology Development Co., LTD., China). Briefly, the piezoelectric effect of PLLA is achieved by means of the molecular structure of the material and the ordered arrangement of the crystals [22]. 1 g of PLLA was dissolved in 5 mL of dichloromethane, and the product of chemical reaction was transferred to a medical syringe. Electrospinning parameters: positive voltage 1 5 kV; fluid feeding speed 1.5 mL/h; type of needle 23G; spinning distance 15 cm. After obtaining the electro spun film, the nanofibrils were obtained by pulverizing and dispersing in the grinder.

Nanoliposomes loaded with drugs were obtained by thin film hydration [23]. Briefly, 60 mg lecithin, 20 mg cholesterol, and 1.0 mg IL-17 inhibitor were dissolved in 30 mL chloroform. Then, the organic solvent was evaporated completely at 35 °C (for about 1 h) to obtain the lipid film attached to the bottom of the round-bottom flask. And 3 mL of redistilled water was added to the flask and decomposed using ultrasound at 25 °C for 20 min completely dissolve the film in water. The product was the micron-sized bilayer of liposomes. To prepare the liposomes with smaller particle size, the 5-min strong probe ultrasonic solution (60 single pulse per min, 130 W) was used.

From our previous study [24], we found that PLGA–PEG–PLGA triblock copolymers can be synthesized by ring opening copolymerization of LA and GA with PEG under the catalytic activity of $Sn(Oct)_2$. The specific steps in the synthesis were as follows: First, PEG (0.01 mol) was dissolved in water, and LA and GA were added without oxygen. Subsequently, the remaining water was removed at 80 °C. After melting all of the monomers, $Sn(Oct)_2$ (0.2 wt %) was added and the mixture was stirred at 150 °C for 12 h under argon protection. At the end of the reaction, the product was added to water at 80 °C, and washed three times. And then the PLGA–PEG–PLGA powder was obtained by lyophilization. Finally, 4 % PLGA–PEG–PLGA and 2.5 % nanoparticles were dissolved in water and stirred for 4 h at 25 °C to obtain the nanocomposite hydrogels.

2.4. Characterization of injectable hydrogels

I) The morphology of electro spun films and nanofibrils was observed by scanning electron microscopy (SEM) (Sirion 200, FEI). II) The piezoelectric properties of the PLLA were examined by an oscillograph (TBS1000C, Tektronix). III) The size of liposomes and the zeta potential difference were accurately measured by dynamic light scattering (DLS) (Zetasizer Nano S, Malvern, UK). IV). The shape of liposomes and Nanoparticles composed of triblock polymers were observed using a transmission electron microscope (TEM) (F200X G2, FEI). V) The storage modulus and loss modulus of the hydrogel system were measured by the rheometer (Mars40, Haake).

2.5. Sequencing of mRNA

After extracting total RNA from the samples, rRNA was removed using Prokaryote-rRNA Removal Kit, and the mRNA was enriched. The enriched mRNA was reverse-transcribed into double-stranded cDNA. After repairing the double ends of the cDNA, a library was constructed via PCR amplification with splicing. Sequencing of the cDNA library was performed on an Illumina HiseqTM 2500/4000 by Gene Denovo Biotechnology Co., Ltd (Guangzhou, China). Bioinformatic analysis was performed using Omicsmart, which is a real-time interactive online platform for data analysis (http://www.omicsmart.com).

2.6. Western blot

Protein samples to be tested were prepared and protease inhibitors were added. The samples were then added to the polyacrylamide gel (SDS-PAGE) and subjected to electrophoresis. After electrophoresis, proteins from SDS-PAGE were transferred to PVDF membranes, and then incubated with skim milk. Membranes were incubated with primary antibodies against the target proteins (IL-17A: GB11110-1, Servicebio, 1:1000; Osterix: GB111900-100, Servicebio, 1:1000; RUNX-2: GB13264-50, Servicebio, 1:1000; CXCL16: GB111441-100, Servicebio, 1:1000; CCL7: ab228979, Abcam, 1:1000). The membranes were incubated overnight at 4 °C, washed, and then incubated for 4 h with secondary antibody (GB23303, Servicebio, 1:3000). After chemical color development, the data were read by chemiluminescence instrument (CLINX-6100).

2.7. Elisa test

The IL-17 Elisa kit (No. SP12224) was purchased commercially from Wuhan Saipei Biotechnology Co., LTD. The femoral head tissue of rats was mashed with normal saline, centrifuged at 1000×*g* for 10 min, and the supernatant was removed. 50 μl of the each sample to be tested was added to the reaction well. 50 μl of biotin-labeled antibody was added and incubated at 37 °C for 1 h. After washing, 50 μl of avidin-HRP was added to each well and incubated at 37 °C for 30 min. And then 50 μl of color developing agent were added to each well, mixed with gentle shaking, and incubated at 37 °C for 10 min, and avoid light. Finally, 50 μl of termination solution was added and the results were determined immediately. The OD values of each well were determined at a wavelength of 450 nm.

2.8. Mitochondrial respiratory chain experiments

Oxygen Consumption Rate (OCR) test kit (No. 103015-100, Agilent Technologies) was purchased from Junli Biotechnology Co., LTD. OCR was determined by measuring changes in dissolved oxygen content in the medium surrounding the cells using the Seahorse energy metabolism analyzer (No. XFe24, Agilent Technologies). During measurements, cells were placed in the presence of specific oxygen consuming reagents such as thiazoles. These agents will interact with the mitochondrial respiratory chain in the cell, leading to changes in the rate of oxygen consumption. The Seahorse energy metabolism analyzer calculated the OCR of cells by measuring the changes in oxygen consumption reagents and dissolved oxygen content in the medium surrounding the cells.

2.9. Flow cytometry

The flow apoptosis kit (No. CA1020) was purchased commercially from Beijing Solarbio Science & Technology Co., LTD. The treated cells were resuspended in binding buffer to a concentration of approximately 1 × 10^6 cells/mL. Appropriate amount of Annexin V-FITC (the

concentration recommended in the instructions) was added and after mixing, the mixture was incubated at 25 °C in the dark for 15–20 min. PI dye was added to a final concentration of 5 μg/mL and the incubation was continued for 5–10 min. Immediately after completion of incubation, analysis was performed using a flow cytometer.

2.10. Animal experiment

The animal experiment for this study were approved by the Ethics Committee of the Second Affiliated Hospital of Zhejiang University School of Medicine (No. 2024-227). The rat model of steroid-induced osteonecrosis of the femoral head was prepared by injecting glucocorticoid at a dose of 0.8 mg twice a week into the buttocks of each rat. In the control group, normal saline could be injected into the buttocks. The model was successfully established after 6 weeks of continuous injection.

2.11. Tissue sections and H&E staining

Rat femoral head tissue blocks were decalcified, embedded in paraffin, and then cut into thin sections (usually 4–6 μm in thickness) using a microtome. Paraffin was removed by treatment with xylene over a series of concentration gradients. The hydration process was carried out through a series of concentration gradient alcoholic solutions. The sections were placed in hematoxylin solution for 5 min to stain the nuclei. A rapid treatment was passed through a 1 % hydrochloric acid alcohol solution for a few seconds to remove excess hematoxylin. After washing, the sections were immersed in a weakly alkaline solution to allow the color of the nuclei to change from dark blue to bright blue. Subsequently, the sections were stained in eosin staining solution for 2 min. After completion of staining, the sections were again dehydrated through a series of concentration gradient alcohol solutions, followed by treatment with xylene to remove water and increase transparency. Finally, a small amount of neutral gum or specialized sealant was dropped onto the sections and covered with a coverslip.

2.12. Immunohistochemical staining

After routine processing of tissue sections, antigen repair was performed using proteinase K. Sections were treated with blocking solution containing serum. Subsequently, sections were treated with the specific primary antibodies (OCN: GB115684-100, Servicebio, 1:1000; OPN: GB11500-100, Servicebio, 1:1000) were incubated overnight at 4 °C. After washing, the plates were incubated for 4 h at room temperature using the secondary antibody. Finally, chromogen was added for color development and observed under a microscope.

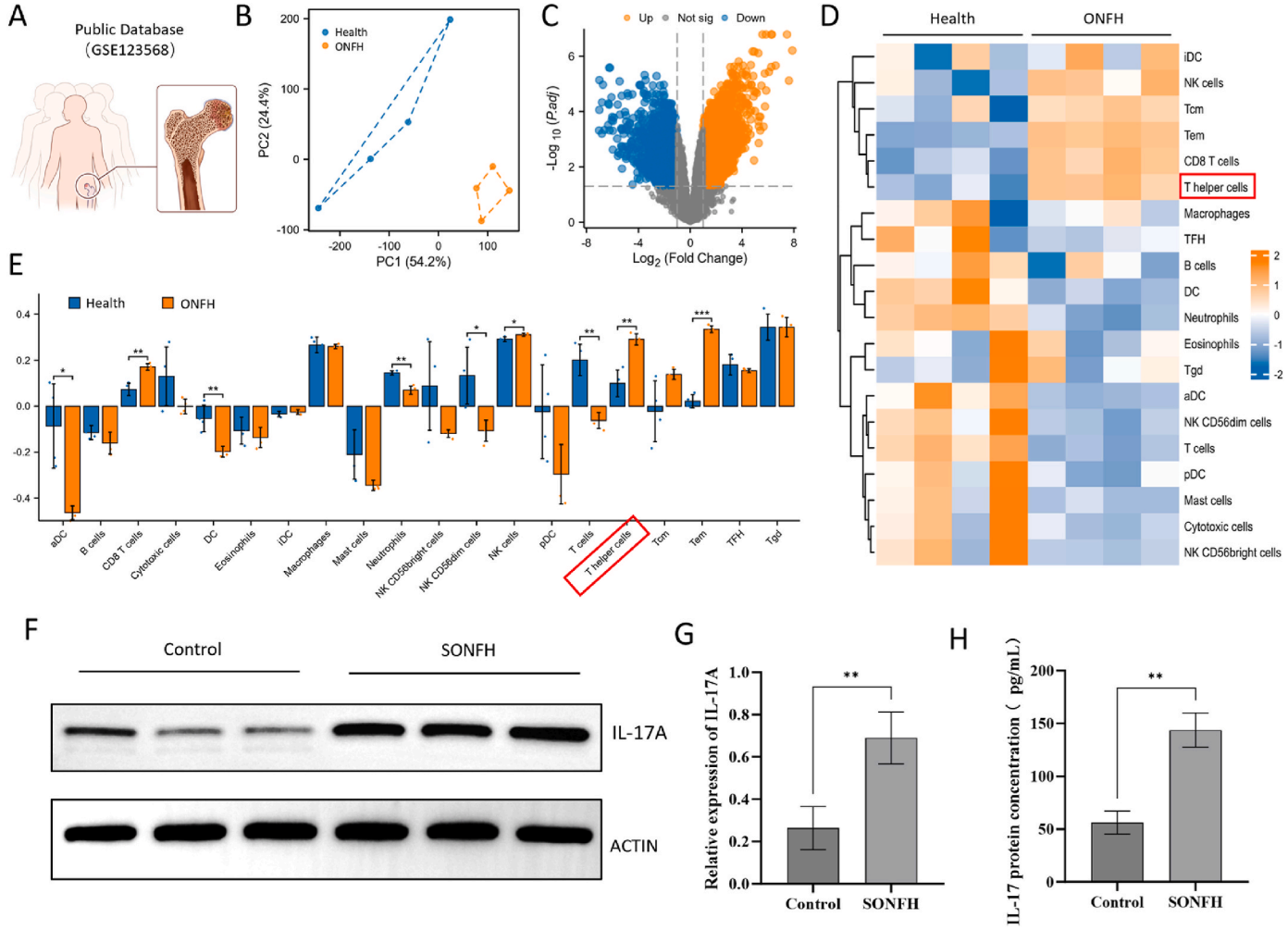

Fig. 1. Immune infiltration in steroid-induced osteonecrosis of the femoral head. A) Sequencing data were obtained from public databases. B) PCA plots of the sequenced samples. C) Differentially expressed genes between healthy and SONFH samples. D) The immune infiltration in SONFH samples was analyzed by ssGSEA (the red box shows the location of Th17 cells). E) Immune infiltration related scores for each immune cell (the red box shows the location of Th17 cells). F) Expression of IL-17A in healthy and SONFH rat femoral head samples. G) Quantitative analysis of Western blot results. H) The content of IL17 in the femoral head was detected by Elisa test. (**$P < 0.01$).

2.13. Statistical analysis

Two-tailed analysis of variance (ANOVA) and *t*-test were used to analyze significant differences between the two groups of samples. Comparisons involving more than two groups were performed using one-way ANOVA with a post-hoc test. All experiments included at least three groups of parallel, repeated samples. Statistical significance was set at $P < 0.05$ and indicated as $^{*}P < 0.05$, $^{**}P < 0.01$, $^{***}P < 0.001$.

3. Results and discussion

3.1. Immune infiltration of Th17 cells during SONFH

To examine the pathological mechanism of SONFH, we mined data from several public databases. Finally, we selected the GSE123568 dataset, which included sequencing data from 40 human femoral head samples, 30 patients with SONFH, and 10 controls (Fig. 1A). We performed bioinformatic analysis of the data. The sample distribution of the PCA plots revealed a clear distinction between the patient data of the SONFH group and that of the Control group (Healthy group) (Fig. 1B). A volcano plot showed that there were 6476 differentially expressed genes in the two groups (fold change >2, $P < 0.05$), of which 4284 were significantly upregulated and 2192 were significantly downregulated (Fig. 1C). Finally, we performed immune infiltration analysis using the single-sample gene set enrichment analysis (ssGSEA) method, and the infiltration of 20 common immune cells was displayed using a heat map (Fig. 1D). The infiltration index of each immune cell is shown using a bar chart, and the difference was statistically analyzed. The results indicated that the immune infiltration of Th17 cells was significantly increased in the lesions of SONFH ($P < 0.01$) (Fig. 1E).

To validate the results of the bioinformatics analysis, a rat model of SONFH was established. The expression of interleukin-17A (IL-17A) in Th17 cells was also assessed. In brief, we constructed the SONFH model by injecting glucocorticoids into the buttock of rats. After the model was successfully constructed, the femoral heads of rats were taken to extract protein for subsequent experiments. The IL-17A content of rat femoral head samples was measured using western blotting (Fig. 1F) and semi-quantitative analysis was performed (Fig. 1G). The results indicated that the IL-17A levels were significantly higher at the lesion site of SONFH compared with that in the Control group. An ELISA kit was used to measure the IL-17 content of the samples. The results indicated that IL-17 levels in the lesions of rats with SONFH was 143.77 pg/mL, which was significantly higher compared with that of the Control group ($P < 0.001$) (Fig. 1H).

Taken together, a large number of Th17 cells infiltrated the lesion site during SONFH, and a large amount of IL-17 was secreted, which had a significantly negative effect on the physiological activity of the stem cells in the lesion, thus affecting the repair of the lesion by stem cells. This may be one of the most important pathological mechanisms of SONFH.

3.2. Characterization and function of injectable hydrogels

To construct an injectable hydrogel system with an electrical stimulation function, we used electrospinning technology to prepare PLLA into electrospun films with piezoelectric effects and then fabricated the PLLA into nanofibrils using a crusher (Fig. 2A). Images of the successfully fabricated electrospun films and nanofibrils are shown in Fig. 2B and C. We evaluated the piezoelectric properties of PLLA, and the results indicated that under the stimulation of ultrasound, the PLLA material generated a micro voltage of 200 mV (Fig. 2D). Finally, the morphology of the electrospun films and nanofibrils was observed through scanning electron microscopy (Fig. 2E and F). To endow injectable hydrogels with a capacity for chemical regulation, we constructed drug-loaded liposomes using thin-film hydration. Transmission electron microscopy revealed that the liposome had a relatively uniform particle size and a perfect shell-core structure, which is important for efficient drug delivery (Fig. 2G and H). In addition, the nanoliposomes loaded with drug showed a good sustained drug release performance within about 2 weeks (**Extended Data** Fig. 1).

Next, we used the unique properties of the PLGA-PEG-PLGA triblock polymer to construct injectable hydrogel carriers (**Extended Data** Fig. 2). Briefly, the PLGA-PEG-PLGA nanoparticles moved freely in the liquid at room temperature, and the hydrogel adopted a liquid shape, which could accommodate the piezoelectric nanofibers and the drug-loaded liposomes. When the hydrogel system was injected into the body, the nanoparticles consisting of PLGA-PEG-PLGA were arranged into a cord-like structure via temperature stimulation, thus transforming the hydrogel system from a liquid to a solid state (Fig. 2I). The liquid-to-solid-state performance of the hydrogel was subsequently verified. Based on these results, at room temperature, the liquid level of both the simple PLGA-PEG-PLGA hydrogel and the hydrogel system changed from tilted to horizontal after the sample bottle was tilted, indicating that both were liquid. However, at 37 °C, the liquid level remained tilted after the sample bottle was tilted, whether it was the simple PLGA-PEG-PLGA hydrogel or the hydrogel system. Over time, the temperature decreased and the liquid level gradually changed from tilted to horizontal. This indicated that both groups were successfully converted to a solid state at 37 °C (Fig. 2J). Finally, we characterized the injectable hydrogel system. The nanoparticles formed using PLGA-PEG-PLGA were subjected to transmission microscopy (Fig. 2K) and the particle size statistics (Fig. 2L) and zeta potential (**Extended Data** Fig. 3) were obtained using DLS. Based on the results, the nanoparticles formed using PLGA-PEG-PLGA were uniformly distributed at room temperature and the particle size was relatively uniform. Subsequently, we used a rheometer to scan the hydrogel at different temperatures under a fixed strain and oscillation frequency (Fig. 2M). At approximately 37 °C, the hydrogel system exhibited a higher storage modulus compared with the dissipation modulus. The ability of the injectable hydrogel system to become solid *in vivo* was also verified.

3.3. Sequencing results of stem cells with electrical stimulation

To verify the regulatory effect of the physical method (electrical stimulation) of the injectable hydrogel on stem cells, we performed mRNA sequencing on the stem cells that received electrical stimulation. After treatment with glucocorticoids, untreated cells were designated the “Control group,” whereas treated cells were designated the “Treatment group.” From the sample distribution shown in the PCA plot, there was a clear distinction between the Control and Treatment groups (Fig. 3A). A volcano plot revealed 3690 differentially expressed genes in the two groups of data (fold change >2, $P < 0.05$), of which 1302 genes were significantly upregulated and 2388 genes were significantly downregulated (Fig. 3B). We performed a cluster analysis on some of the differentially expressed genes and displayed them on a heat map (Fig. 3C). Through GO analysis, we enriched the differentially expressed genes, and the top 10 GO terms with the highest scores are shown using a circle diagram. They included: Molecular function (GO: 0005488; GO: 0005515), Cellular components (GO: 0005634; GO: 0005622), and Biological processes (GO: 002402; GO: 0007049) (Fig. 3D). We also performed KEGG enrichment analysis on the differentially expressed genes, and the top 10 KEGG terms with the highest enrichment scores were shown using a circle diagram. They included: Cellular processes (KO: 04110; KO: 04218), Genetic information process (KO: 03030; KO: 03430), Metabolism (KO: 00100), Human disease (KO: 05206; KO: 05200), and Environmental information process (KO: 04350; KO: 04668) (Fig. 3E).

To determine the effect of electrical stimulation on stem cell repair in focal tissue, we organized the GO terms related to osteogenesis, in which the enrichment of “Osteoblasts differentiation” and “Regulation of osteoblast differentiation” was significantly different (Fig. 3F). This indicates that electrical stimulation can effectively promote the osteogenic

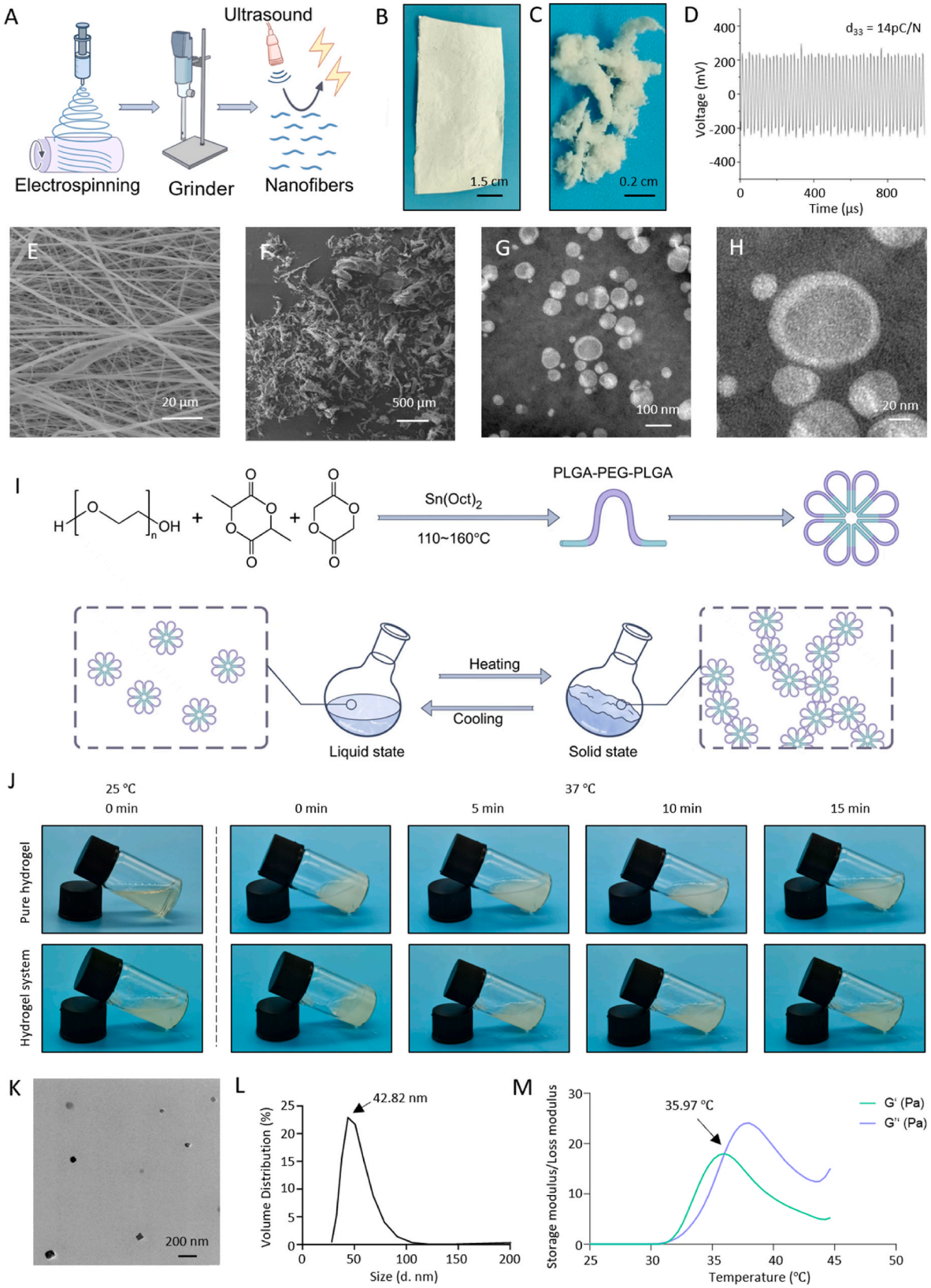

Fig. 2. Preparation and characterization of injectable hydrogel systems. A) Schematic representation of the preparation of nano staple fibers with piezoelectric property. B) The photograph of the electrospun film. C) The photograph of a nano staple fiber. D) Piezoelectric effect of nano staple fiber. E) The scanning electron microscopy of electrospun film. F) The scanning electron microscopy of nano staple fiber. G) The transmission electron microscopy of nanoliposomes. H) High-fold transmission electron micrographs of nanoliposomes. I) Schematic representation of the PLGA-PEG-PLGA triblock polymer constituting an injectable hydrogel. J) The injectable hydrogel showed a transition from solid to liquid with the change of temperature. K) The transmission electron micrographs of a nanoparticle constructed of a triblock polymer. L) Particle size distribution of nanoparticles constructed from triblock polymers. M) Rheological data for injectable hydrogel systems (G': storage modulus, G'': loss modulus).

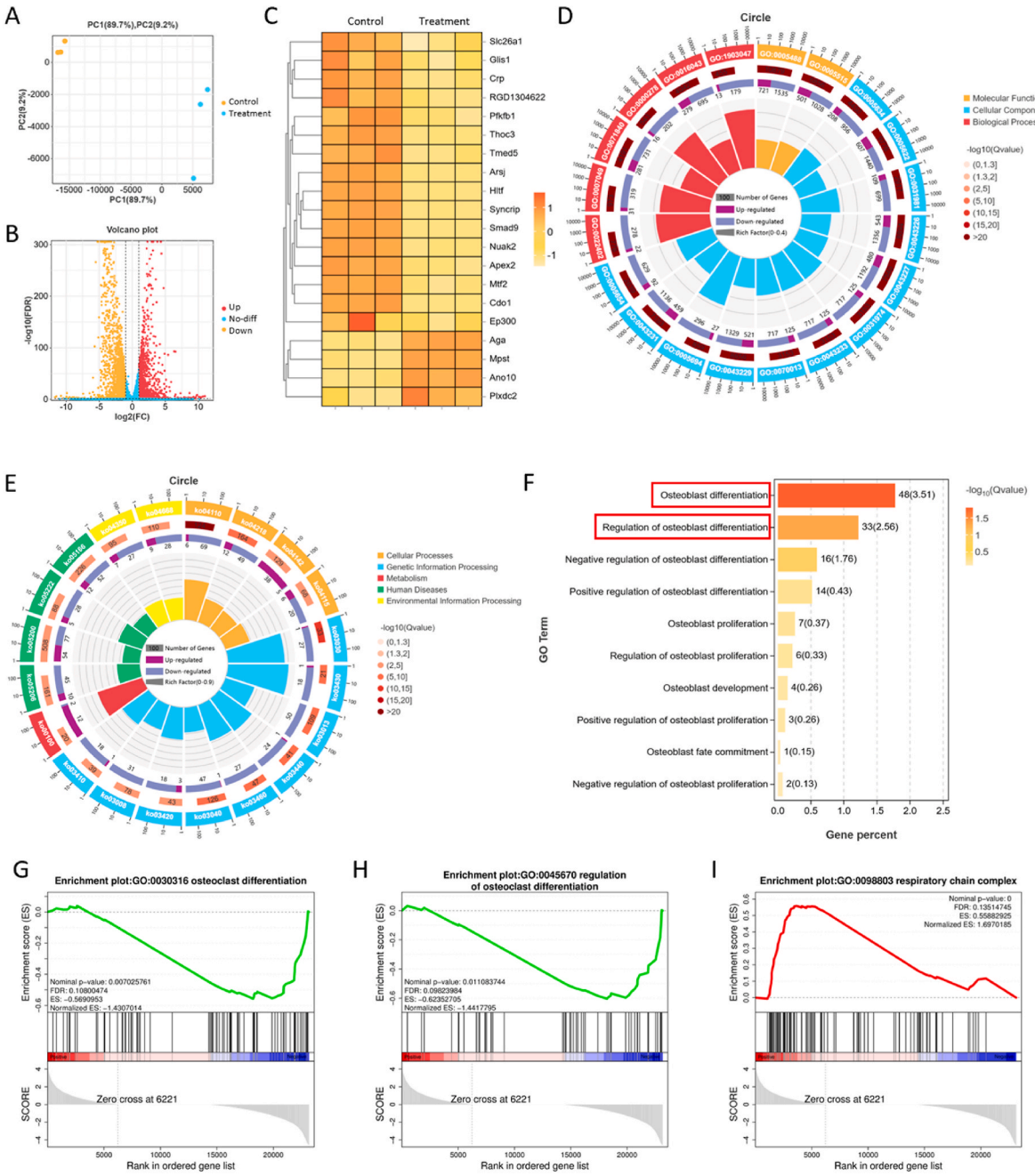

Fig. 3. mRNA sequencing data after electrical stimulation of stem cells. A) PCA plots of electrically stimulated and control samples. B) Differentially expressed genes in stem cells after electrical stimulation. C) Heat map shows representative differentially expressed genes. D) Enrichment of differentially expressed genes in different GO items. E) Enrichment of differentially expressed genes in different KEGG items. F) GO items related to osteogenic or osteoclast differentiation of stem cells (the red box indicates the GO items to focus on). G) GSEA Enrichment of differentially expressed genes in "Osteoclasts differentiation" item. H) GSEA Enrichment of differentially expressed genes in "Regulation of osteoclast differentiation" item. I) GSEA Enrichment of differentially expressed genes in "Respiratory chain complex" item.

differentiation of stem cells, thereby repairing the focal tissue. Moreover, ssGSEA revealed a negative normalized enrichment score (NES) for "Osteoclasts differentiation" and "Regulation of osteoclast differentiation" (Fig. 3G and H). This indicates that the core genes associated with these two terms are significantly under expressed. This is further evidence that electrical stimulation can promote osteoblast differentiation and inhibit osteoclast differentiation. Additionally, a large number of differentially expressed genes were enriched in mitochondria-related GO items (**Extended Data** Fig. 4). And the NES value of "Respiratory chain complex" was positive (Fig. 3I). This indicates that the core genes involved in mitochondrial respiratory function were significantly highly expressed. Electrical stimulation may improve the function of the mitochondrial respiratory chain in stem cells.

3.4. Electrical stimulation promotes osteogenic differentiation and mitochondrial respiratory chain function in stem cells

The mRNA sequencing results suggested that the electrical stimulation of the injectable hydrogel promotes osteogenic differentiation of stem cells and increases cell viability by enhancing mitochondrial respiratory chain function; however, these results still need to be verified through further experiments. First, a rat model of SONFH was

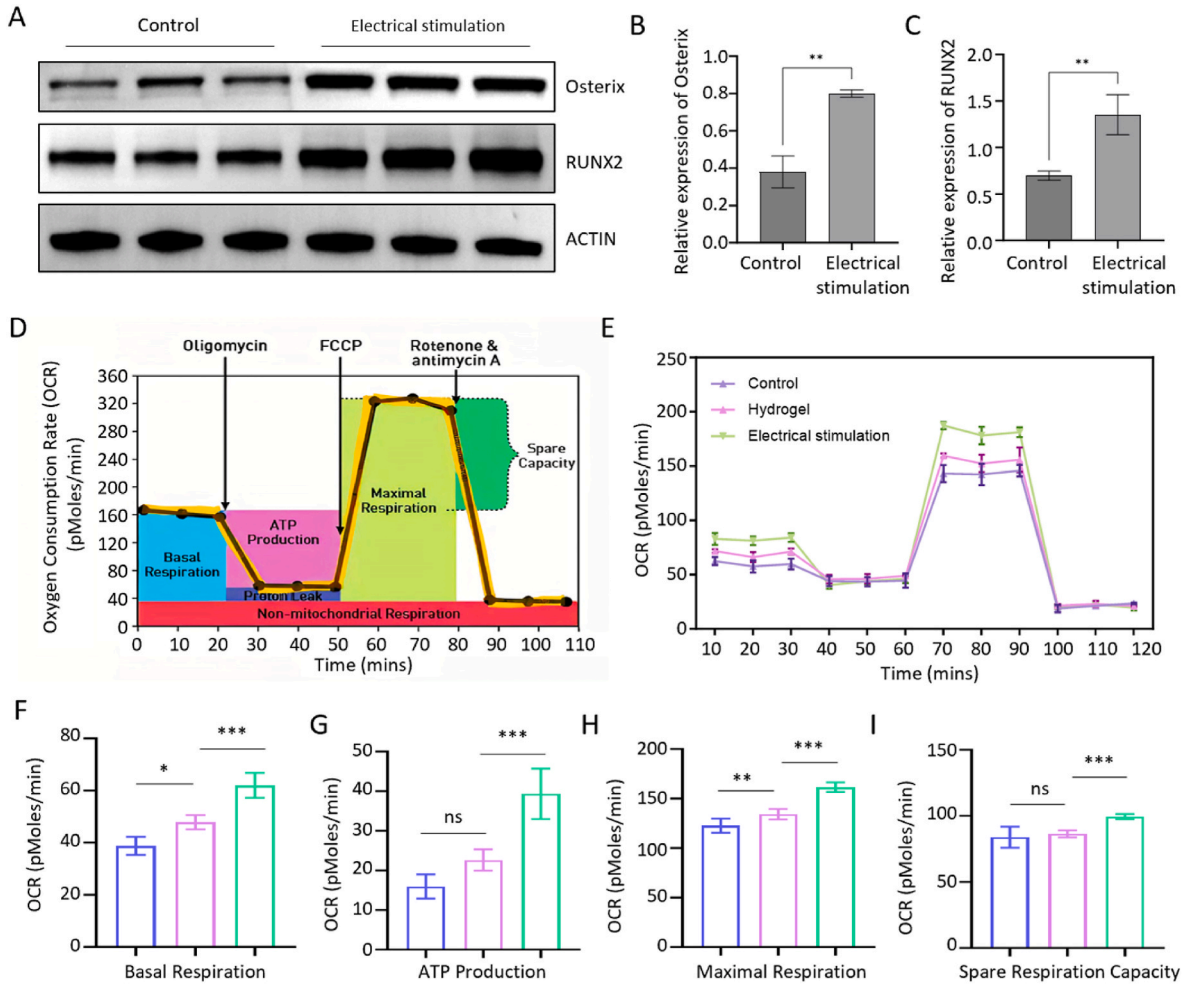

Fig. 4. Electrical stimulation promoted osteogenic differentiation and mitochondrial respiratory chain function of stem cells. A) Expression of osteogenic differentiation-related proteins in stem cells. B-C) Quantitative analysis of Osterix protein and RUNX2 protein expression. D) Schematic representation of the mitochondrial respiratory chain function test. E) Mitochondrial respiratory chain function curves. F) Quantitative analysis of the basal respiration function of mitochondria. G) Quantitative analysis of the ATP production function of mitochondria. H) Quantitative analysis of the maximal respiration function of mitochondria. I) Quantitative analysis of the spare respiration capacity of mitochondria. (ns: no significant; $*P < 0.05$; $**P < 0.01$; $***P < 0.001$).

established based on the above methods. The Control group was untreated, whereas the experimental group was injected with hydrogel and stimulated using ultrasound to obtain electrical stimulation. Subsequently, the femoral head lesions of the two groups were extracted, and the osteogenic differentiation potential of the stem cells in the lesions under electrical stimulation was evaluated using western blot analysis (Fig. 4A), following which the results were semi quantitatively analyzed (Fig. 4B and C). The results demonstrated that the markers of osteogenic differentiation in stem cells, Osterix and Runx-2, were significantly upregulated following electrical stimulation compared with the Control group. This indicates that electrical stimulation of the injectable hydrogel can promote the osteogenic differentiation of stem cells at the lesion site, thereby promoting the repair of femoral head necrosis. To verify the effect of the injectable hydrogel on the mitochondrial respiratory chain function in the stem cells, the respiratory chain function was examined before and after electrical stimulation (Fig. 4D). The MSCs were cocultured with the hydrogel, designated as the "Hydrogel group," and the hydrogel was stimulated using ultrasound to induce a microcurrent, which was designated the "Electrical stimulation group." Finally, the mitochondrial respiratory chain function of each group was detected, and a respiratory function curve was generated (Fig. 4E). The results indicated that the basal respiratory function of the MSCs was significantly enhanced by treatment with hydrogel and electrical stimulation (Fig. 4F). Additionally, electrical stimulation significantly increased mitochondrial ATP production (Fig. 4G). The abundant production of ATP provides energy for the proliferation and differentiation of stem cells. The maximal respiration (Fig. 4H) and spare respiration capacity (Fig. 4I) were significantly increased via electrical stimulation, indicating that the mitochondrial potential of the MSCs was significantly improved. This suggests a potential increase in respiratory efficiency in a lesion microenvironment. Overall, electrical stimulation of the injectable hydrogel can effectively promote the osteogenic differentiation of MSCs and the function of the mitochondrial respiratory chain to provide sufficient energy for the activities of MSCs.

3.5. *Physical and chemical synergy for regulating Th17 cell immune infiltration*

To further examine the effect of electrical stimulation on Th17 immune infiltration, we further analyzed the mRNA sequencing data. The results indicated that a large number of differentially expressed genes were enriched in GO terms related to chemotaxis, such as chemotaxis, lymphocyte chemotaxis, and cell chemotaxis (Fig. 5A). We selected GO terms related to lymphocyte and T-cell chemotaxis and screened out a total of 11 related differentially expressed genes. Of these, WNK-1, Ccl-7, Cxcl-16, and Adam-17 were highly expressed in the Control group, and their expression was significantly downregulated following electrical stimulation (Fig. 5B). The chemokines, Cxcl-16 and Ccl-7, play an

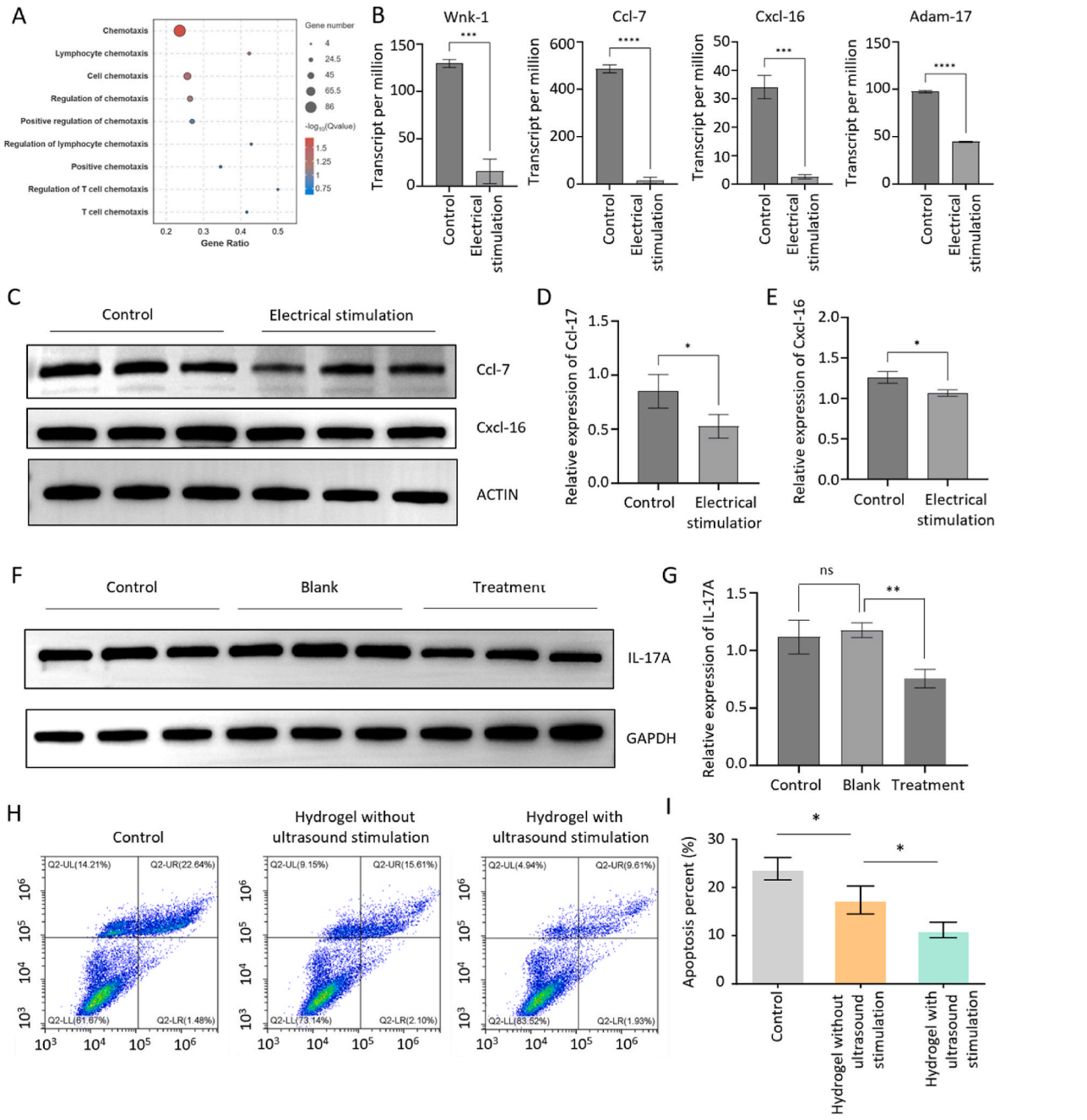

Fig. 5. Physical and chemical methods synergistically regulate the negative effects of Th17 cells. A) GO items related to T lymphocyte immune infiltration. B) Differentially expressed genes related to Th17 cell chemotaxis. C) The expression of Ccl-7 and Cxcl-16 chemokines were determined by Western blot test. D) Quantitative analysis of the expression of Ccl-7. E) Quantitative analysis of the expression of Cxcl-16. F) Effects of chemical method on IL-17A synthesis by Th17 cells. G) Quantitative analysis of the expression of IL-17A. H) Flow cytometry was used to detect the apoptosis of stem cells. I) Quantitative analysis of stem cell apoptosis. (*$P < 0.05$; **$P < 0.01$; ***$P < 0.001$).

important role in the immune infiltration of Th17 cells. In subsequent experiments, we established a rat model of SONFH based on the above methods. The Control group was untreated, whereas the experimental group was injected with hydrogel and stimulated using ultrasound to obtain electrical stimulation. To validate the test results, the expression of Cxc-16 and Ccl-7 proteins was measured at the lesion site (Fig. 5C) and analyzed semi quantitatively (Fig. 5D and E). The results indicated that the expression of Cxcl-16 and Ccl-7 in the lesion area of the rats treated with electrical stimulation was significantly decreased, which was consistent with the sequencing results. Subsequently, to verify that Cxcl-16 and Ccl-7 promote the migration of Th17 cells, we designed the Transwell migration assay (**Extended Data** Fig. 5A). The migration ability of Th17 cells was reflected by counting the cells in the lower chamber of the Transwell plate. The results showed that the number of Th17 cells in the Chemokines group was significantly increased compared with the Control group without chemokine stimulation (**Extended Data** Fig. 5B). This indicates that Cxcl-16 and Ccl-7 can promote the migration ability of Th17 cells. Taken together, the injectable hydrogel effectively reduces the synthesis and secretion of Cxcl-17 and Ccl-7 from MSCs through electrical stimulation, thereby inhibiting the immune infiltration of Th17 cells and improving the pathological microenvironment of SONFH.

Subsequently, the effect of the hydrogel chemical method on Th17 regulation was verified. Th17 cells were used as a Control group, a Blank

group cocultured with the hydrogel system without drug loading, and the Treatment group cocultured with the hydrogel system with drug loading. IL-17 protein was measured in each group (Fig. 5F). The synthesis of IL-17 protein in the Treatment group was significantly lower than that in the Control and Blank groups (Fig. 5G). These results indicate that the chemical regulation of the injectable hydrogel system can effectively inhibit the synthesis of IL-17 by Th17 cells, thereby blocking the side effects of Th17 cells on MSCs.

To further verify the effect of Th17 cells on MSC cells, we established a coculture system of Th17 cells and MSCs. Similar to the above experiments, the cells without the hydrogel system were used as the Control group, and the cells cocultured with the drug-loaded hydrogel system were used as the Hydrogel without ultrasound stimulation group, and ultrasonic treatment was applied to generate electrical stimulation, which was set as Hydrogel with ultrasound stimulation group. Apoptosis of the MSCs in each group after treatment was assessed using flow cytometry (Fig. 5H). The results indicated that after coculture with Th17 cells, MSCs in the Control group exhibited a large number of apoptotic because of the influence of IL-17. However, apoptosis of MSCs in the Hydrogel without ultrasound stimulation group was significantly lower compared with that in the Control group because of the chemical regulation of the hydrogel system. At the same time, the apoptosis rate of MSCs in Hydrogel with ultrasound stimulation group was significantly lower than that in Hydrogel without ultrasound stimulation group (Fig. 5I). These results indicate that the physical and chemical co-regulation of the injectable hydrogel system can effectively inhibit the apoptosis of MSCs induced by Th17 cells, and the effect is better than that of any single regulation method.

3.6. *Injectable hydrogels for the treatment of SONFH in rats*

Finally, we determined the efficacy of the injectable hydrogel for the treatment of SONFH using a rat model (**Extended Data** Fig. 6). Healthy rats were considered the Control group and rats with SONFH induced by glucocorticoid treatment represented the Hormone group. Rats injected with hydrogel without drug loading and ultrasonic treatment were

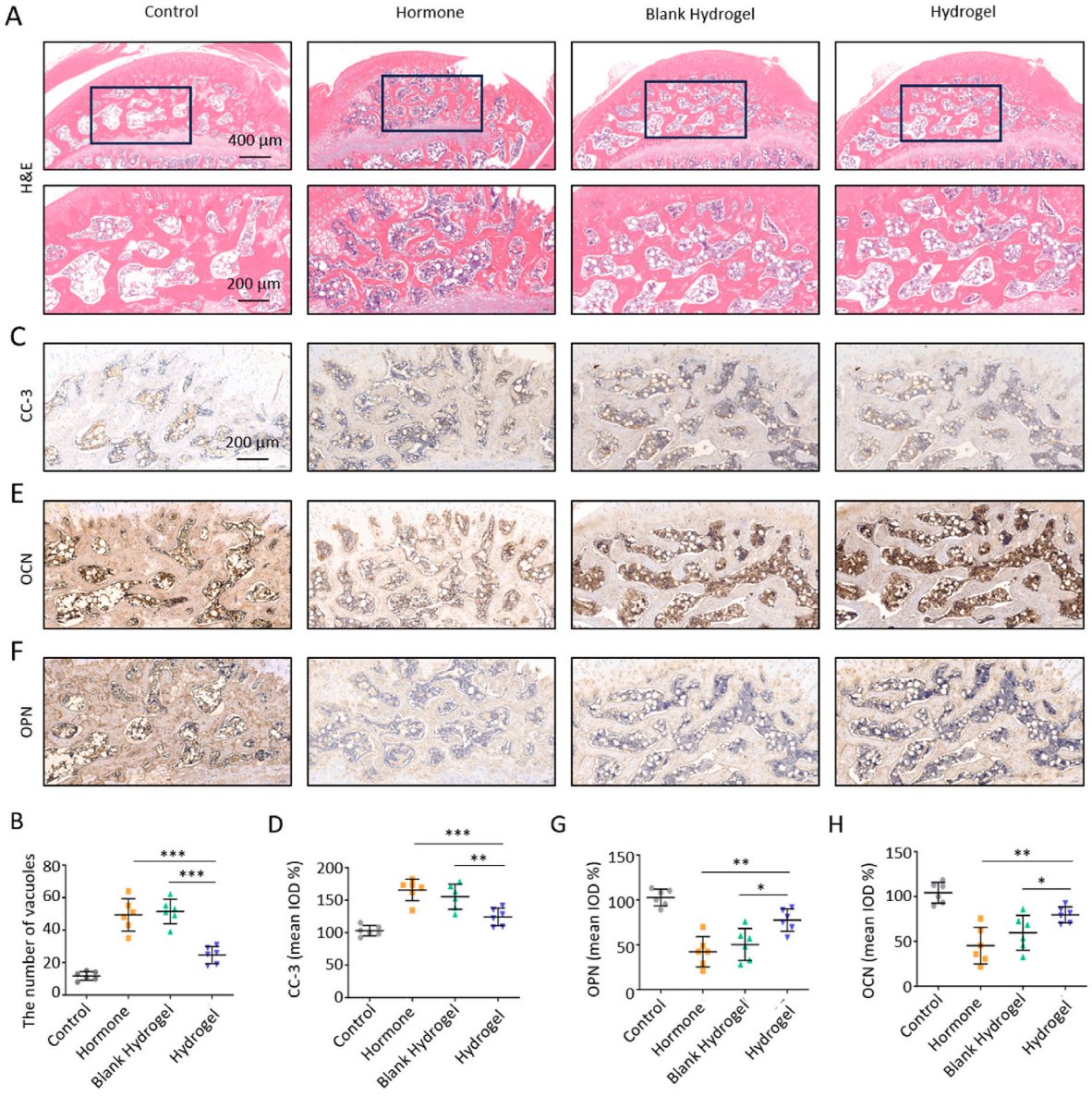

Fig. 6. Injectable hydrogel system for treatment of SONFH rats. A) Hematoxylin and eosin staining of the rat femoral head. B) Quantitative analysis of the number of vacuoles in the femoral head. C) Immunohistochemical staining for cleaved caspase-3 in the femoral head. D) Quantification of cleaved caspase-3 expression. E) Immunohistochemical staining for OPN in the femoral head. F) Immunohistochemical staining for OCN in the femoral head. G) Quantification of OPN expression. H) Quantification of OCN expression. (*$P < 0.05$; **$P < 0.01$; ***$P < 0.001$).

considered the Blank Hydrogel group. Finally, the Hydrogel group was established by injecting hydrogel loaded with drugs and applying a microcurrent. After completing the treatment, we evaluated rat femoral head progression by preparing sections and H&E staining. The results indicated that the number of vacuoles in the trabecular bone of the femoral head in the steroid group increased significantly. This was caused by the apoptosis of osteoblasts and the degradation of the extracellular matrix, indicating that the SONFH model was successful. Compared with the Blank Hydrogel group, the number of femoral head vacuoles in the Hydrogel group was significantly decreased, indicating that the injectable hydrogel system effectively ameliorated the progression of SONFH (Fig. 6A and B).

To detect apoptosis in the necrotic tissue of the femoral head, we performed cleaved caspase-3 immunohistochemical staining on the rat femoral head sections (Fig. 6C). Semiquantitative analysis of the staining revealed that compared with the Control group, the value of CC-3 in the Hormone and Blank Hydrogel groups was significantly increased, indicating that the microenvironment of the SONFH lesions exhibited a large number of apoptotic cells (including osteoblasts and MSCs). However, the CC-3 value of the Hydrogel group was significantly lower compared with that of the Blank Hydrogel group, indicating that the injectable hydrogel effectively inhibited stem cell apoptosis at the lesion site (Fig. 6D). Finally, the effect of the injectable hydrogel system on the repair and regeneration of SONFH lesions was evaluated. We performed immunohistochemical staining for osteopontin (OPN) and osteocalcin (OCN) (Fig. 6E–H). OPN and OCN are markers of stem cell osteogenic differentiation during the repair of lesions, so they can reflect recovery. The results showed that compared with the Hormone group and the Blank Hydrogel group, the OPN and OCN values in the Hydrogel group were significantly increased. These results indicate that MSCs significantly improve the repair ability of SONFH lesions regulated by the injectable hydrogel system. Taken together, the injectable hydrogel system can inhibit the progression of femoral head lesions in SONFH rats, inhibit the apoptosis of MSCs in the lesions, and promote the repair and regeneration of the lesions.

4. Conclusion

In this study, we examined the relationship between SONFH and immune infiltration, focusing on the impact of Th17 cell immune infiltration on the progression of SONFH. We developed an injectable hydrogel system to enhance the physiological activity of MSCs while mitigating the negative effects of Th17 cell immune infiltration through synergistic physical and chemical regulation, effectively ameliorating SONFH. This system represents a promising biomaterial for treating SONFH. Additionally, our findings on the correlation between SONFH progression and immune infiltration offer valuable insights for developing new treatments. The physical and chemical coordination measures established in this study may also inspire future advancements in biomaterials.

With the development of materials science, medical biomaterials gradually play an important role in medical treatment [25–27]. However, our injectable hydrogel system has tremendous advantages over traditional medical biomaterials. Although our disease model is SONFH, the hydrogel system can be extended to various diseases. Electrical stimulation is universally effective to cells. By exploring the effects of electrical stimulation on various lesions and various cells and the cellular and molecular mechanisms, and then using targeted chemical regulation methods to assist, we can effectively reduce the adverse factors of lesion cells, or improve the ability of cells to promote the repair of lesions. Therefore, the hydrogel system we constructed has great potential for expansion. At the same time, this study also has some limitations, such as insufficient exploration of the regulatory mechanism of immune infiltration. The infiltration of a variety of immune cells (e.g., NK cells, CD8 T cells) in SONFH lesions has been significantly increased, and the effect of these immune cells on SONFH progression still needs to be further explored in the future.

CRediT authorship contribution statement

Zherui Fu: Writing – original draft, Methodology, Investigation, Formal analysis. **Yiwen Xu:** Methodology, Investigation, Formal analysis, Data curation. **Fangqi Xu:** Methodology, Investigation, Formal analysis, Data curation. **Haoyu Zhou:** Methodology, Investigation. **Na Lin:** Methodology, Investigation, Formal analysis, Data curation. **Ning Zhang:** Visualization, Validation, Supervision, Project administration. **Feng Lin:** Writing – review & editing, Project administration, Methodology, Investigation, Funding acquisition.

Declaration of competing interest

The authors declare that they have no known competing financial interests or personal relationships that could have appeared to influence the work reported in this paper.

Acknowledgments

This work was financially supported by was supported by grants from National Natural Science Foundation of China (grant No. 52403207), Zhejiang Provincial Natural Science Foundation of China (grant No. LY23H060008), National Health Commission Scientific Research Fund & Zhejiang Provincial Medical and Health Major Science and Technology Plan Project (grant No. WKJ-ZJ-2428) and National Natural Science Foundation of China (grant No. 81972514).

Appendix A. Supplementary data

Supplementary data to this article can be found online at https://doi.org/10.1016/j.mtbio.2025.101511.

Data availability

Data will be made available on request.

References

[1] A. Wang, M. Ren, J. Wang, The pathogenesis of steroid-induced osteonecrosis of the femoral head: a systematic review of the literature, Gene 671 (2018) 103–109.
[2] T. Kubo, K. Ueshima, M. Saito, M. Ishida, Y. Arai, H. Fujiwara, Clinical and basic research on steroid-induced osteonecrosis of the femoral head in Japan, J. Orthop. Sci. 21 (2016) 407–413.
[3] X. Qi, Y. Zeng, Biomarkers and pharmaceutical strategies in steroid-induced osteonecrosis of the femoral head: a literature review, J. Int. Med. Res. 43 (2015) 3–8.
[4] Y. Kuroda, Y. Okuzu, T. Kawai, K. Goto, S. Matsuda, Difference in therapeutic strategies for joint-preserving surgery for non-traumatic osteonecrosis of the femoral head between the United States and Japan: a review of the literature, Orthop. Surg. 13 (2021) 742–748.
[5] J. Zhang, S. Guo, M. Tao, D. Yu, C.K. Cheng, Automatic planning and geometric analysis of the drilling path in core decompression surgery for osteonecrosis of the femoral head, Comput. Methods Progr. Biomed. 247 (2024) 108059.
[6] C. Wei, M. Yang, K. Chu, J. Huo, X. Chen, B. Liu, et al., The indications for core decompression surgery in patients with ARCO stage I-II osteonecrosis of the femoral head: a new, comprehensive prediction system, BMC Muscoskel. Disord. 24 (2023) 242.
[7] Z. Fu, Y. Lai, Y. Zhuang, F. Lin, Injectable heat-sensitive nanocomposite hydrogel for regulating gene expression in the treatment of alcohol-induced osteonecrosis of the femoral head, APL Bioeng. 7 (2023) 16107.
[8] F. Lin, L. Xiang, L. Wu, Y. Liu, Q. Jiang, L. Deng, et al., Positioning regulation of organelle network via Chinese microneedle, Sci. Adv. 10 (2024) eadl3063.
[9] F. Lin, Z. Wang, L. Xiang, L. Wu, Y. Liu, X. Xi, et al., Transporting hydrogel via Chinese acupuncture needles for lesion positioning therapy, Adv. Sci. 9 (2022) e2200079.
[10] C. Liu, C. Wang, Y. Liu, J. Huang, W. Xu, J. Li, et al., Selenium nanoparticles/carboxymethyl chitosan/alginate antioxidant hydrogel for treating steroid-induced osteonecrosis of the femoral head, Int. J. Pharm. 653 (2024) 123929.
[11] F. Lin, Z. Wang, L. Xiang, L. Wu, Y. Liu, X. Xi, et al., Transporting hydrogel via Chinese acupuncture needles for lesion positioning therapy, Adv. Sci. 9 (2022) e2200079.

[12] Y. Zhuang, F. Lin, L. Xiang, Z. Cai, F. Wang, W. Cui, Prevented cell clusters' migration via microdot biomaterials for inhibiting scar adhesion, Adv. Mater. 36 (2024) e2312556.
[13] F. Lin, Y. Li, W. Cui, Injectable hydrogel microspheres in cartilage repair, Biomed. Technol. 1 (2023) 18–29.
[14] W. Fang, P. Peng, K. Lin, F. Xiao, W. He, M. He, et al., M6a methylation modification and immune infiltration analysis in osteonecrosis of the femoral head, J. Orthop. Surg. Res. 19 (2024) 183.
[15] J. Zhao, X. Zhang, J. Guan, Y. Su, J. Jiang, Identification of key biomarkers in steroid-induced osteonecrosis of the femoral head and their correlation with immune infiltration by bioinformatics analysis, BMC Muscoskel. Disord. 23 (2022) 67.
[16] R. Yu, J. Zhang, Y. Zhuo, X. Hong, J. Ye, S. Tang, et al., ARG2, MAP4K5 and TSTA3 as diagnostic markers of steroid-induced osteonecrosis of the femoral head and their correlation with immune infiltration, Front. Genet. 12 (2021) 691465.
[17] N.S. Adapala, R. Yamaguchi, M. Phipps, O. Aruwajoye, H. Kim, Necrotic bone stimulates proinflammatory responses in macrophages through the activation of toll-like receptor 4, Am. J. Pathol. 186 (2016) 2987–2999.
[18] P. Liu, Y. Gao, P. Luo, H. Yu, S. Guo, F. Liu, et al., Glucocorticoid-induced expansion of classical monocytes contributes to bone loss, Exp. Mol. Med. 54 (2022) 765–776.
[19] Z. Li, B. Yang, X. Weng, G. Tse, M. Chan, W. Wu, Emerging roles of MicroRNAs in osteonecrosis of the femoral head, Cell Prolif. 51 (2018).
[20] H. Wu, H. Dong, Z. Tang, Y. Chen, Y. Liu, M. Wang, et al., Electrical stimulation of piezoelectric BaTiO3 coated Ti6Al4V scaffolds promotes anti-inflammatory polarization of macrophages and bone repair via MAPK/JNK inhibition and OXPHOS activation, Biomaterials 293 (2023) 121990.
[21] P. Xiao, X. Han, Y. Huang, J. Yang, L. Chen, Z. Cai, et al., Reprogramming macrophages via immune cell mobilized hydrogel microspheres for osteoarthritis treatments, Bioact. Mater. 32 (2024) 242–259.
[22] S. Zhang, H. Zhang, J. Sun, N. Javanmardi, T. Li, F. Jin, et al., A review of recent advances of piezoelectric poly-L-lactic acid for biomedical applications, Int. J. Biol. Macromol. 276 (2024) 133748.
[23] F. Lin, Z. Wang, L. Xiang, L. Deng, W. Cui, Charge-guided micro/nano-hydrogel microsphere for penetrating cartilage matrix, Adv. Funct. Mater. 31 (2021).
[24] Y. Zhuang, X. Yang, Y. Li, Y. Chen, X. Peng, L. Yu, et al., Sustained release strategy designed for lixisenatide delivery to synchronously treat diabetes and associated complications, ACS Appl. Mater. Interfaces 11 (2019) 29604–29618.
[25] Y. Wang, J. Guo, X. Cao, Y. Zhao, Developing conductive hydrogels for biomedical applications, Smart Med 3 (2024) e20230023.
[26] Z. Luo, Y. Wang, Y. Xu, J. Wang, Y. Yu, Modification and crosslinking strategies for hyaluronic acid-based hydrogel biomaterials, Smart Med 2 (2023) e20230029.
[27] Molliard S. Gavard, J. Bon Bétemps, B. Hadjab, A. Ghazal, M. Badi, M. Cerrano, Stabilized composition of 26 mg/mL of high molecular weight HA for subcutaneous injection to improve skin quality, Plast. Aesth. Res. 9 (2022) 52.